

ANALYSIS OF COMPLEX APPARENT RESISTIVITY DATA CONJUGATING SPECTRAL INDUCED POLARIZATION AND ELECTROMAGNETIC COUPLING

Taíla Crístia Souza Sant'Ana¹ and Edson Emanuel Starteri Sampaio²

ABSTRACT. The induced polarization characteristic is to provide geophysical and geological information via geoelectric parameters, making possible mineral discrimination in the scope of mineral exploration. Although represents one of the main noises in measurements of this method, electromagnetic coupling between current and potential electrodes also contributes to the understanding of the geological scenario. Thus, the most appropriate way to deal with such data is an integrated study of these two phenomena, taking into account their particularities. Forward modelling and Gauss-Newton inversion of the mutual impedance in the frequency domain provide the analysis of the complex apparent resistivity considering both spectral induced polarization and electromagnetic coupling for homogeneous and one-dimensional, non-polarizable and polarizable Earth models. Besides synthetic data, this new approach was applied to data from the Copper District of Vale do Curaçá, Bahia, Brazil. The results reveal the ability of the method to distinguish between induction, dominant at the highest frequencies, and induced polarization, which varies with depth and frequency. It also may constitute a basis for mineral discrimination with the analysis of analogous circuit parameters, a fundamental tool in the search for metallic targets in mineral exploration.

Keywords: forward modelling, geophysical inversion, electromagnetic method, mineral exploration.

RESUMO. A polarização induzida espectral se destaca por fornecer diversas informações geofísico-geológicas através dos parâmetros geoeletricos, viabilizando a discriminação mineral no âmbito da exploração mineral. Embora constitua um dos principais ruídos nas medidas desse método, o acoplamento eletromagnético entre eletrodos de corrente e potencial também auxilia na compreensão do cenário geológico. Dessa forma, a maneira mais adequada de lidar com tais dados espectrais é o estudo integrado desses dois fenômenos, levando em conta suas particularidades. A modelagem direta e a inversão Gauss-Newton da impedância elétrica mútua no domínio da frequência proporcionam a análise da resistividade complexa aparente considerando tanto a polarização induzida espectral como o acoplamento eletromagnético para modelos de terra homogênea e uni-dimensional, polarizável e não-polarizável. Além do dado sintético, essa nova abordagem foi aplicada a dados reais do Distrito Cuprífero do Vale do Curaçá, Bahia, Brasil. Os resultados revelam a capacidade do método em distinguir o efeito indutivo, dominante nas mais altas frequências, e a variação da polarização induzida com a profundidade e frequência. Isso constitui um estudo base para a discriminação mineral por meio da análise de parâmetros de circuitos análogos, uma ferramenta fundamental na investigação de alvos em exploração mineral.

Palavras-chave: modelagem direta, inversão geofísica, método eletromagnético, exploração mineral.

¹Universidade Federal da Bahia, Rua Barão de Jeremoabo, s.n., Salvador, Bahia, Brazil, 40170-115. Phone: +55(71) 99985-5853 – E-mail: taila_cristia@hotmail.com

²Universidade Federal da Bahia, Rua Barão de Jeremoabo, s.n., Salvador, Bahia, Brazil, 40170-115. Phone: +55(71) 3283-8603 – E-mail: starteri@ufba.br

INTRODUCTION

Electromagnetic coupling (EMC) between current and potential electrodes is a phenomenon which yields a dependence of the modulus and the phase of electrical resistivity with frequency. EMC plays a dual role in geophysical surveys because it is a source of spurious anomalies in spectral induced polarization (SIP) data (Millett, 1967) but it helps to improve the analysis of the variation of electrical parameters in controlled source electromagnetic (CSEM) data (Wynn & Zonge, 1977).

The characterization of EMC as a noise caused the emergence of several techniques of minimization and removal of its effect in SIP measurements both in time and frequency domains (Pelton et al., 1978; Çaglar, 2000; Fullagar et al., 2000; Xiang et al., 2002). Furthermore, the removal of its effect may allow the analysis of the role of SIP in mineral discrimination (Sampaio et al., 1998).

We analyze field and synthetic data of both SIP and EMC. Our objective is to understand the behavior of the complex apparent resistivity function (ρ_a), produced by the combination of the two phenomena, as the frequency of the source and the spacing between transmitter and receiver dipoles vary. This procedure aims to establish a basis for mineral discrimination by means of the analysis of the parameters of Barreto & Dias (2014) in different geological situations.

The method employed to achieve this goal follows three steps: (1) 1-D forward modelling of the EMC mutual impedance data in frequency domain for a dipole-dipole array assuming a homogeneous and polarizable Earth (Mocitaiba et al., 2017), integrated with the model of Barreto & Dias (2014); (2) implementation of the inversion algorithm of the mutual impedance data based on the forward modelling in order to obtain ρ_a and to interpret it in terms of both EMC and SIP effects; (3) application of inversion to SIP field data from the Vermelhos, Baixa Funda and Sussuarana mineral deposits of the Copper District of Vale do Curaçá, Bahia, Brazil. Our approach differs from previous analysis, which didn't take into account the EMC (Sampaio et al., 1998).

Forward Modeling of Mutual Impedance

The forward modelling is based on the followings equations (Mocitaiba et al., 2017), which determine the mutual impedance in the frequency domain under the quasistatic condition. In this context, a dipole-dipole array is employed at (x_0, y_0, z_0) over a homogeneous and an η -layered Earth, with the following settings: dipole length equal to $2L$, separation between the

centers of the transmitting and receiving dipoles equal to $2(n + 1)L$, $n = 1, 2, 3, \dots, 7$ and $L = 25$ m.

In this sense, the mutual impedance for a homogeneous Earth is given by

$$Z(z_0, \omega) = \frac{\Delta V(z_0, \omega)}{I(\omega)} \approx -\frac{i\mu_0\omega}{4\pi} \int_0^{+\infty} \left(\frac{2}{\lambda + \alpha_1} G_x(\lambda) + \frac{2}{\lambda \kappa_1^2} G_z(\lambda) \right) e^{\lambda z_0} \lambda d\lambda, \quad (1)$$

where $\Delta V(z_0, \omega)$ and $I(\omega)$ are, respectively, the electric potential and the electric current in the frequency domain, μ_0 is the magnetic permeability, λ is the radial wavenumber, $i = \sqrt{-1}$, $\alpha_1 = \sqrt{\lambda^2 - \kappa_1^2}$, $\kappa_1^2 = \frac{-i\mu_0\omega}{\rho_1}$, and ρ_1 is the electric resistivity of the half-space.

In the case of an η -layered Earth, the mutual impedance is expressed by

$$Z(z_0, \omega) = \frac{\Delta V(z_0, \omega)}{I(\omega)} \approx -\frac{i\mu_0\omega}{4\pi} \int_0^{+\infty} \left[\frac{2}{\lambda + \hat{\alpha}_1} G_x(\lambda) + \frac{2}{\lambda^2} \left(\frac{1}{\lambda + \hat{\alpha}_1} + \frac{\hat{\beta}_1}{\rho_1 \kappa_1^2} \right) G_z(\lambda) \right] e^{\lambda z_0} \lambda d\lambda, \quad (2)$$

where

$$\hat{\alpha}_j = \alpha_j \frac{\hat{\alpha}_{j+1} + \alpha_j \tanh(\alpha_j h_j)}{\alpha_j + \hat{\alpha}_{j+1} \tanh(\alpha_j h_j)}, \quad j = 1, 2, \dots, \eta - 1, \quad (3)$$

$$\hat{\alpha}_\eta = \alpha_\eta, \quad \alpha_j = \sqrt{\lambda^2 - \kappa_j^2}, \quad \kappa_j^2 = \frac{-i\mu_0\omega}{\rho_j}, \quad j = 0, 1, 2, \dots, \eta, \quad (4)$$

$$\hat{\beta}_j = \beta_j \frac{\hat{\beta}_{j+1} + \beta_j \tanh(\alpha_j h_j)}{\beta_j + \hat{\beta}_{j+1} \tanh(\alpha_j h_j)}, \quad j = 1, 2, \dots, \eta - 1, \quad (5)$$

$$\hat{\beta}_\eta = \beta_\eta, \quad \beta_0 = \frac{\alpha_0}{i\varepsilon_0\omega}, \quad \beta_j = \alpha_j \rho_j, \quad j = 0, 1, 2, \dots, \eta, \quad (6)$$

ε_0 is the dielectric permittivity of the half-space, ρ_j and h_j are, respectively, thickness and electric resistivity of the j -th layer.

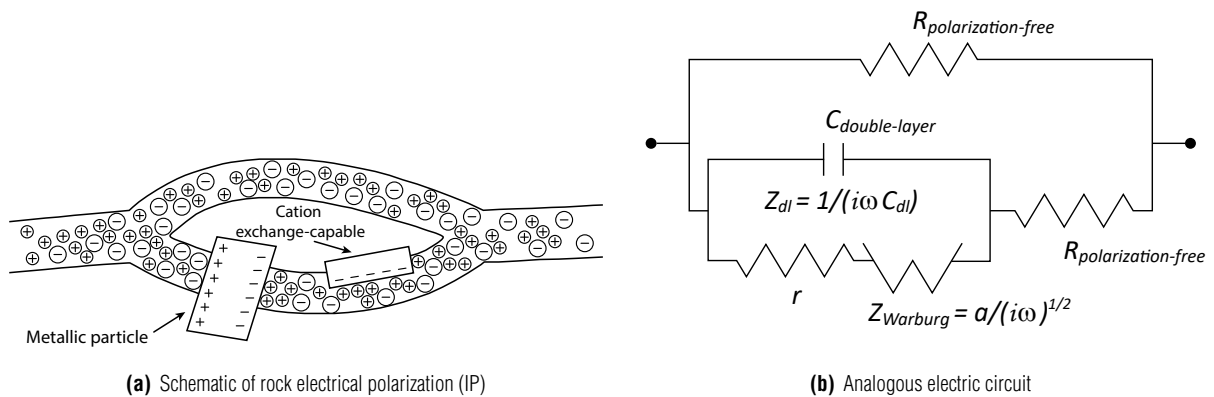


Figure 1 – Principles of the Dias model (Dias, 2000).

In Eqs.(1) and (2), the auxiliary functions $G_x(\lambda)$ and $G_z(\lambda)$ are x and x_0 integrations applied to the Bessel function and defined as

$$G_x(\lambda) = \int_{(2n+1)L}^{(2n+3)L} \int_{-L}^{+L} J_o(\lambda(x-x_0)) dx_0 dx, \quad (7)$$

and

$$G_z(\lambda) = \frac{\partial^2}{\partial x^2} \int_{(2n+1)L}^{(2n+3)L} \int_{-L}^{+L} J_o(\lambda(x-x_0)) dx_0 dx, \quad (8)$$

where J_o is the Bessel function of first kind and 0-th order. While $G_x(\lambda)$ is solved by numeric integration, $G_z(\lambda)$ is determined using

$$\frac{\partial^2}{\partial x^2} = -\frac{\partial^2}{\partial x \partial x_0} \quad (9)$$

which gives

$$G_z(\lambda) = J_0(2\lambda nL) + J_0(2\lambda(n+2)L) - 2J_0(2\lambda(n+1)L). \quad (10)$$

Assuming a complex and frequency dependent resistivity in the case of a polarizable medium, we added the SIP effect to EMC in those equations, by adopting the resistivity model related to the analogous electric circuit represented in Figure 1 and expressed by (Barreto & Dias, 2014)

$$\frac{\rho^* - \rho_\infty}{\rho_0} = \frac{m_W}{1 + (i\omega\tau_W)^{1/2}} + \frac{m_D}{1 + i\omega\tau_D}, \quad (11)$$

where ρ^* is the complex resistivity; ρ_∞ , ρ_0 are resistivity values, respectively, at zero frequency and at a frequency much higher than 1 MHz; τ_W and m_W are, respectively, relaxation time and

chargeability at low frequencies (1 MHz - 10^2 Hz); τ_D and m_D are, respectively, relaxation time and chargeability at higher frequencies (10 kHz - 1 MHz).

This model represents SIP phenomena in rocks by means of an appropriate choice of its parameters, which reflects the petrophysical properties and conducts to studies of mineral discrimination. The values of the parameters adopted are those of the synthetic sample 1 from Barreto & Dias (2014) with 6.5% vol. chalcopyrite disseminated in a matrix consisting of quartz sand.

Complex Apparent Resistivity Estimation

Assuming a uni-dimensional, homogeneous and polarizable Earth model, we have implemented an inversion algorithm to estimate ρ_a employing mutual impedance data for each frequency ω and separation n between source and receiver. To solve this non-linear problem we have used the Gauss-Newton's interactive inversion method involving complex quantities (Menke, 1989; Nocedal & Wright, 2006).

Considering the model parameter as ρ_a and the data as the mutual impedance, the residual between given data, \mathbf{d}_{obs} , and the calculated data, $f(\mathbf{m})$, expressed by

$$\Delta \mathbf{d}(\mathbf{m}) = \mathbf{d}_{obs} - f(\mathbf{m}), \quad (12)$$

is approximated by a first order Taylor's series expansion about the current model \mathbf{m}_k , obtaining

$$\Delta \mathbf{d}(\mathbf{m}_k) \approx \hat{\Delta} \mathbf{d}(\mathbf{m}) = \sum_{i=1}^M \left. \frac{\partial f(\mathbf{m})}{\partial m_i} \right|_{\mathbf{m}_k} (m_i - m_{i,k}) \quad (13)$$

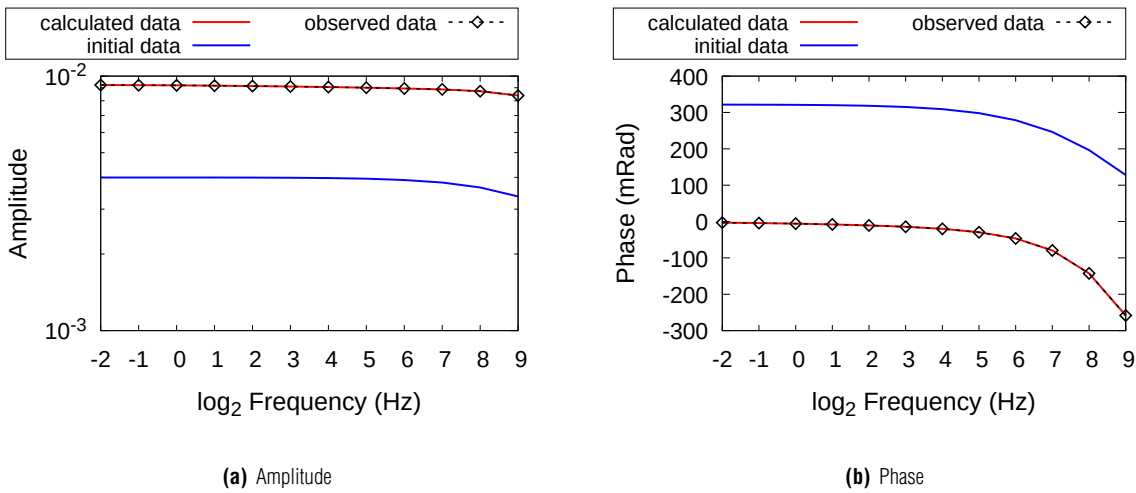


Figure 2 – Example of the result of synthetic data inversion related to spacing $n = 7$ in a 3-layered Earth model with a second polarizable layer, $h_1 = 10$ m, $h_2 = 20$ m, $\rho_1 = 100 \Omega\text{m}$, $\rho_2 = 500 \Omega\text{m}$, and $\rho_3 = 1000 \Omega\text{m}$.

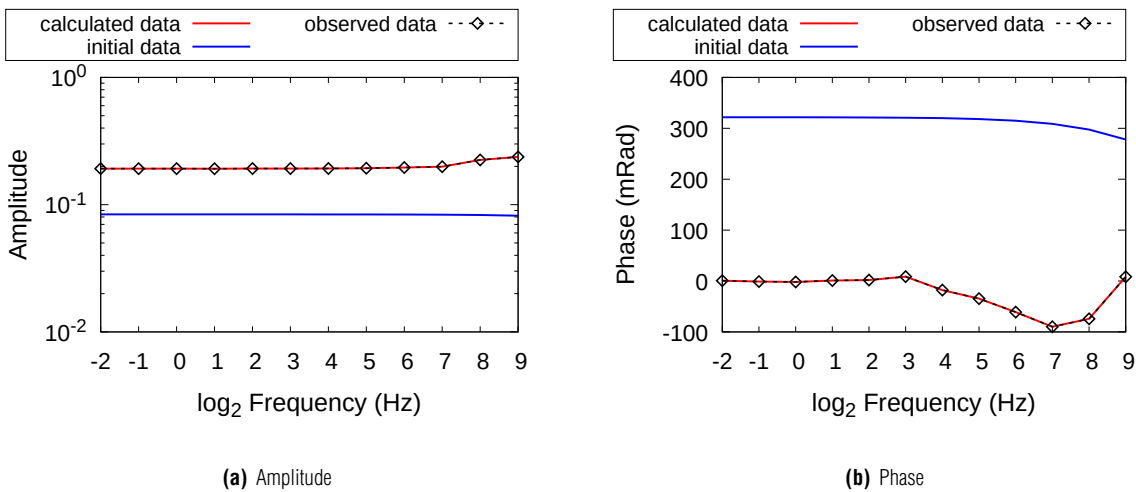


Figure 3 – Example of the result of real data inversion related to spacing $n = 2$ of the profile in the Sussuarana area of the Copper District of Vale do Curuçá.

Seeking to minimize the objective function, $\Phi = \hat{\Delta} \mathbf{d}_k^H \hat{\Delta} \mathbf{d}_k$, we arrive at the following solution of the inverse problem

$$\mathbf{m}_{k+1} = \mathbf{m}_k + (\mathbf{G}_k^H \mathbf{G}_k)^{-1} \mathbf{G}_k^H \Delta \mathbf{d}_k, \quad (14)$$

where H is the Hermitian transpose and \mathbf{G}_k is the derivative matrix of $f(\mathbf{m})$ related to \mathbf{m} or sensibility matrix.

In this inverse problem, data and parameters are unitary and the method converges quickly and leads to a negligible error in both synthetic and real data, as Figures 2 and 3 show respectively.

SYNTHETIC DATA

Mutual impedance and complex apparent resistivity data were analyzed for an eventually polarizable 3-layered Earth model with resistivity values: $\rho_1 = 100 \Omega\text{m}$, $\rho_2 = 500 \Omega\text{m}$, and $\rho_3 = 1000 \Omega\text{m}$; and thicknesses $h_1 = 10$ m and $h_2 = 20$ m.

Figure 4 displays the spectra of phase of mutual impedance. In the case of a non-polarizable half-space, the EMC effect increases with spacing for $f > 16$ Hz. A subtle negative phase shift occurs when polarization is added to any layer for $f < 16$ Hz and the spacing and frequency response is compatible with the depth of polarization. The amplitude presents negligible spectral

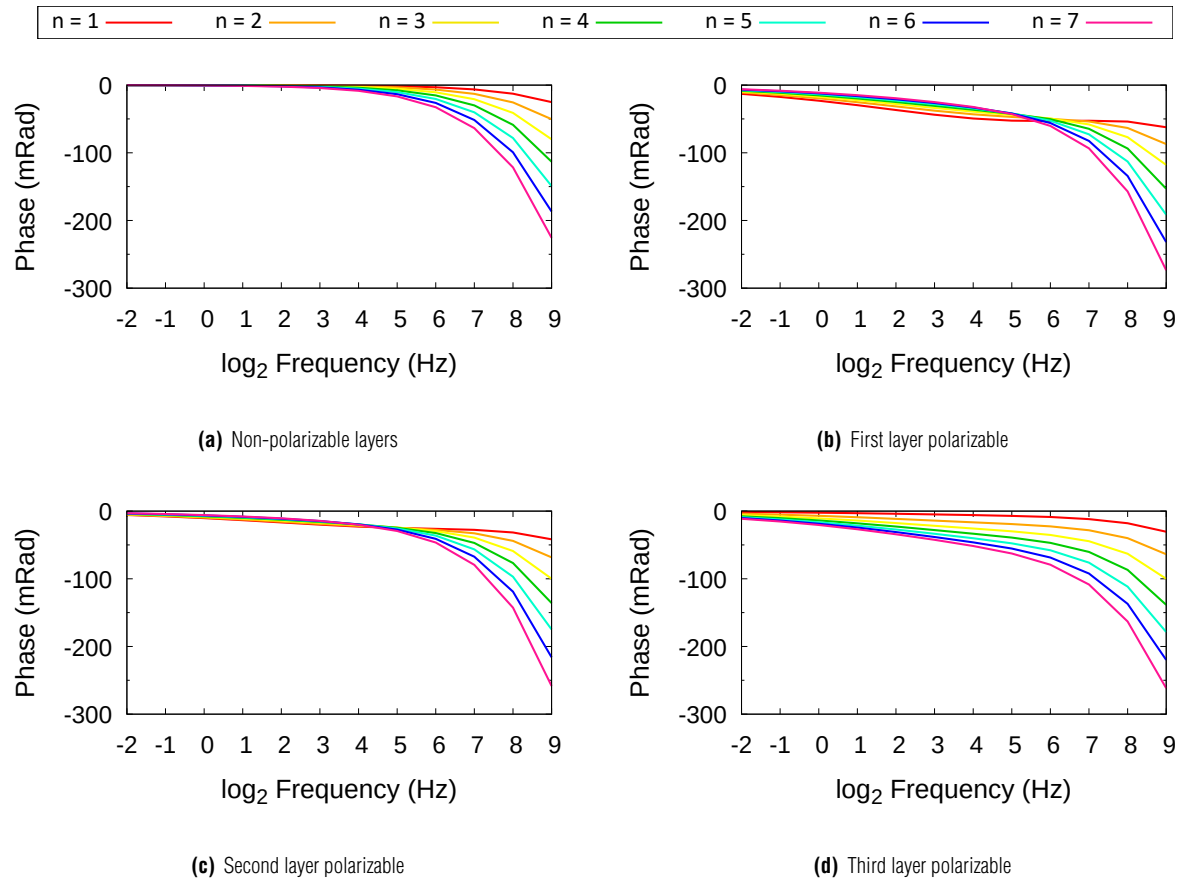


Figure 4 – Spectra of the phase of mutual impedance for an eventually polarizable 3-layered Earth model; $h_1 = 10$ m, $h_2 = 20$ m, $\rho_1 = 100\Omega\text{m}$, $\rho_2 = 500\Omega\text{m}$, and $\rho_3 = 1000\Omega\text{m}$.

variation in the 0.25 Hz to 512 Hz range even with the presence of polarization.

The spectra of phase of ρ_a is shown in Figure 5. When neither layer is polarizable (Figs. 5(a) and 5(b)), the spectral variation in ρ_a are due to EMC effect. As the separation increases, the amplitude reflects the variation of the resistivity with depth. The phase remains close to zero up to 32 Hz, and above this frequency value, the inductive effect produces a negative phase shift proportional to the source-receiver distance.

Assuming a polarizable first layer (Figs. 5(c) and 5(d)), SIP causes a decay of the amplitude with the frequency for all n 's. The phase undergoes a considerable negative displacement for all levels and frequencies, but are more pronounced for $n = 1$ and attenuates as n increases until $n = 7$. If only the second layer is polarizable (Figs. 5(e) and 5(f)), SIP produces a more smooth decay in both amplitude and phase. However, the largest phase changes relative to the non-polarizable case occur for the smaller spacing. For a polarizable basement (Figs. 5(g) and 5(h)),

levels $n = 1$ and $n = 2$ have few changes and the SIP effect is pronounced at the largest distance ($n = 6$ and $n = 7$).

FIELD DATA

We applied the inversion procedure to impedance data of a single transmitter station in three areas with known mineral deposits of the Copper District of Vale do Curaçá: Vermelhos, Baixa Funda and Sussuarana.

Vermelhos

In Vermelhos station (Fig. 6), the amplitude spectrum suggests that resistivity increases with depth, with a variation of more than twenty times between $n = 3$ and $n = 4$. Positive amplitude peaks occur for $n = 3$ to $n = 6$ between 128 Hz and 256 Hz and for $n = 2$ at 64 Hz. This disturbance may be related to a geological discontinuity of limited extent, since it is not recorded in $n = 1$ and $n = 7$. Otherwise, the amplitude is practically constant with frequency.

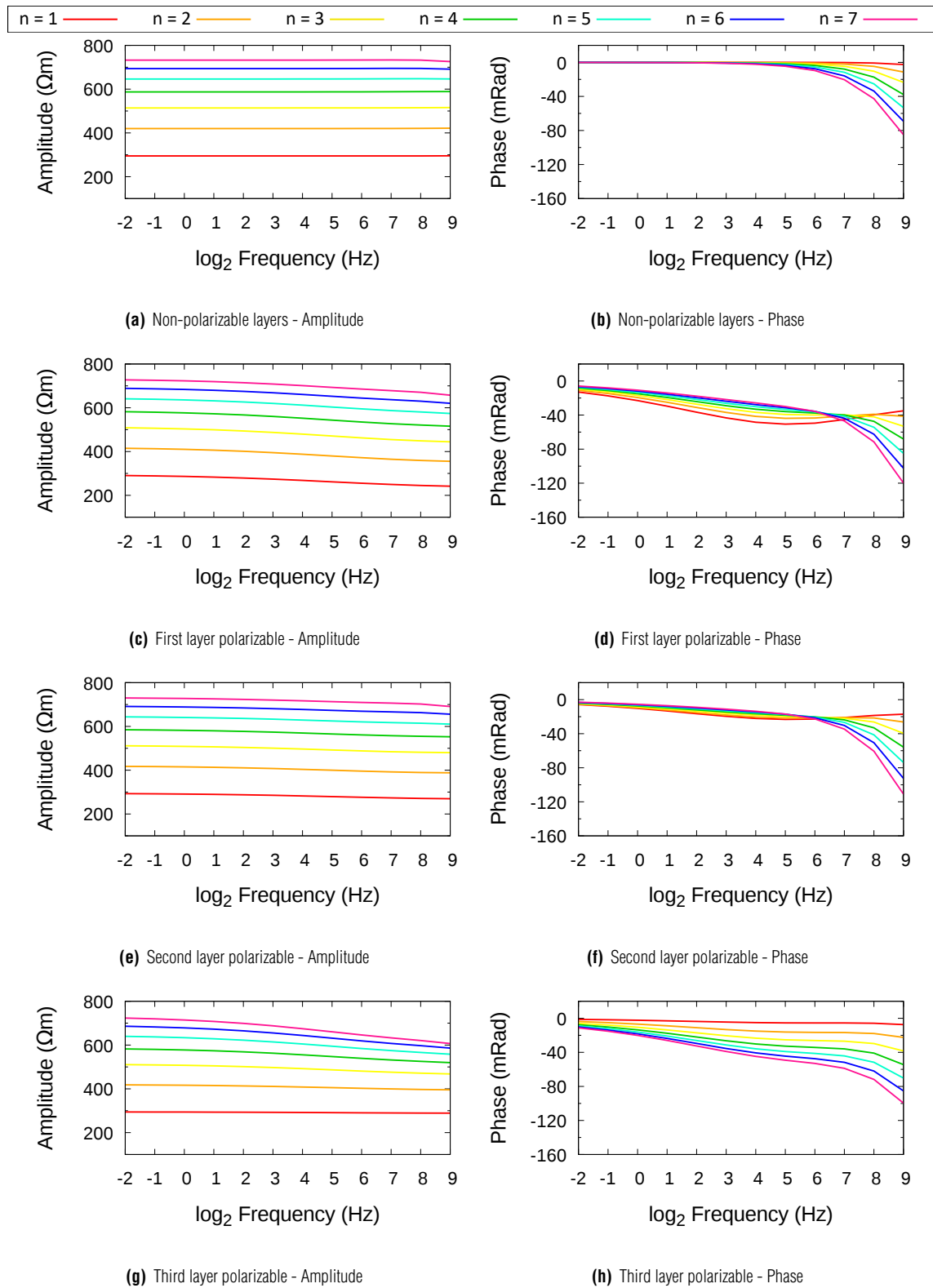


Figure 5 – Spectra of the modulus and phase of ρ_a for an eventually polarizable 3-layered Earth model; $h_1 = 10$ m, $h_2 = 20$ m, $\rho_1 = 100 \Omega\text{m}$, $\rho_2 = 500 \Omega\text{m}$, and $\rho_3 = 1000 \Omega\text{m}$.

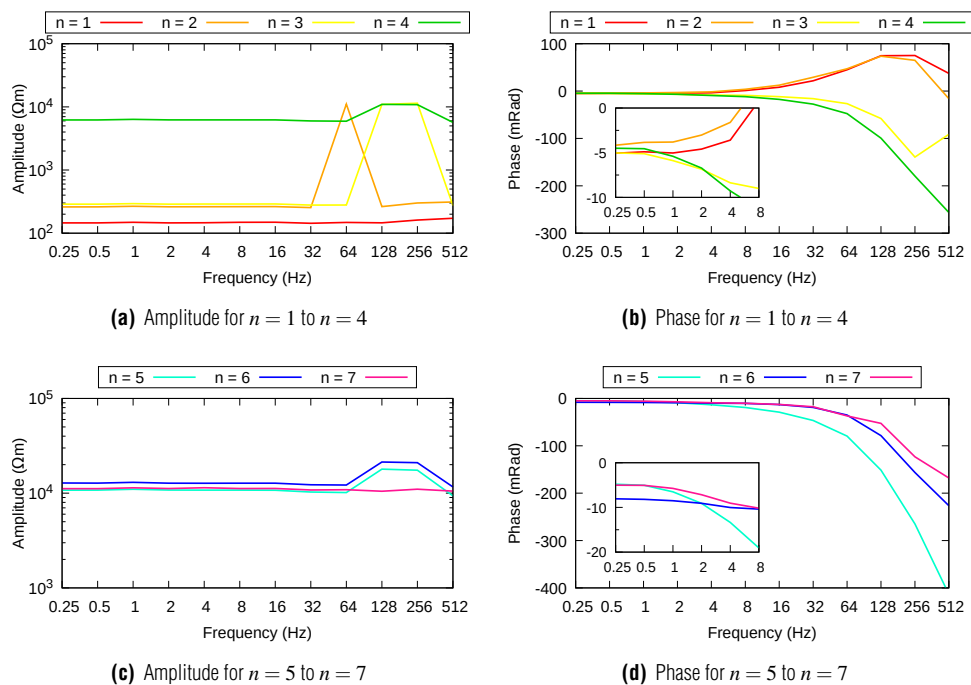


Figure 6 – Spectra of the modulus and the phase of ρ_a for SIP data of one transmitter station of the profile in the Vermelhos area of the Copper District of Vale do Curaçá.

The IP response from 0.25 Hz to 8 Hz causes a subtle negative phase shifts, which is more enhanced for larger n 's. For $n = 1$ and $n = 2$, there is a differential behavior in phase relative to the other n 's, showing a positive phase shift with peak at 128 Hz and 256 Hz, while for the others separations this EM shift is negative with a peak at $f \geq 512$ Hz.

Baixa Funda

In Baixa Funda spectrum (Fig. 7), the amplitude also increases with n and therefore with depth. Likewise, its peaks indicate inhomogeneity between $n = 3$ and $n = 7$. Otherwise, it is approximately constant, with subtle elevations for $n = 1$ and $n = 2$ in $f > 256$ Hz.

The phase spectrum presents similarities with Vermelhos, including a positive phase shift at the highest frequencies for $n = 1$ and $n = 2$, while for the other n 's the combination of IP and EMC causes a negative peak. As to the IP effect in the lower frequencies (0.25 Hz to 8 Hz), the phase decays but reaches little values (< 10 mRad).

Sussuarana

The spectral behavior of the Sussuarana amplitude (Fig. 8) expresses that the resistivity increases with depth, with more

abrupt variations between n equal 1 and 2 and between the n intervals 4 and 5 and 5 and 6.

Up to 64 Hz, the amplitudes are practically constant for all n 's. The curves of $n = 1$ and $n = 2$ show a tiny increase at the higher frequencies. The peaks at 128 Hz and 256 Hz for n between 3 and 6 must be related to lateral discontinuities at intermediate depths. The largest peaks are located in $n = 3$ and $n = 4$.

The phase spectrum, assumed due to IP, shows the most significant variation in Sussuarana. Between 0.25 Hz and 8 Hz, the phase of the levels $n = 3$ to $n = 7$ decays considerably. Since the three largest levels are the most affected, the IP effect may be present at the largest depths. The phase spectrum for $n = 1$ and $n = 2$ show positive phase shifts up to 8 Hz, caused by the resistivity contrast between overburden and the second layer. For $32 \text{ Hz} < f < 256 \text{ Hz}$, the combination of IP and EMC causes negative phase shifts.

CONCLUSION

The mutual impedance data shows that the impedance is strongly masked by the EMC, so that the IP effect is almost undetected by its amplitude and subtly detected by the phase.

Analyzing the complex apparent resistivity of synthetic data, it was possible to note that the amplitude reflects the variation of

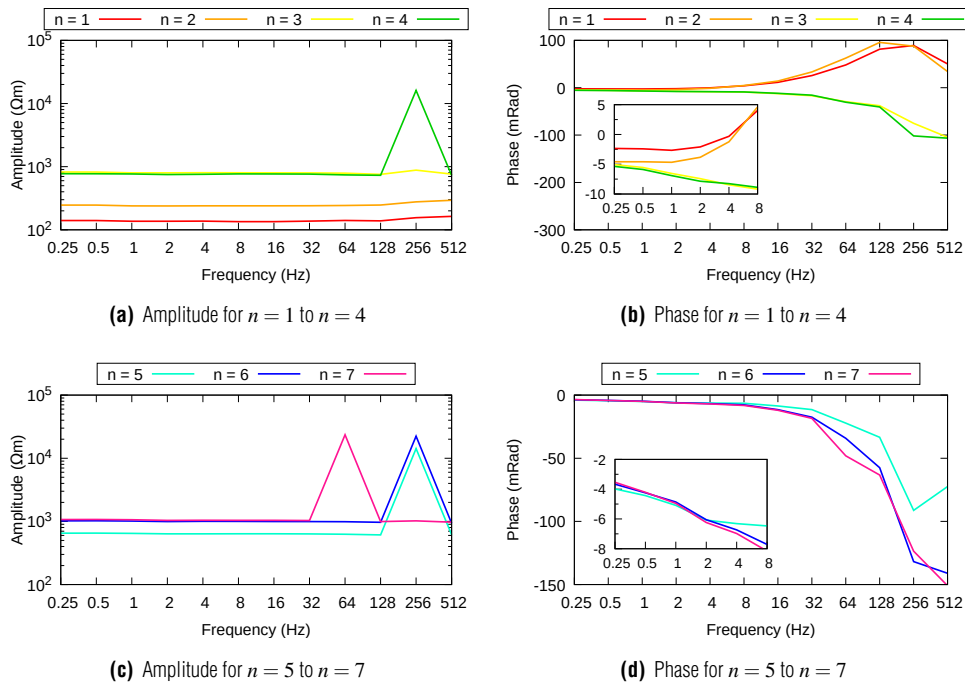


Figure 7 – Spectra of the modulus and the phase of ρ_a for SIP data of one transmitter station of the profile in the Baixa Funda area of the Copper District of Vale do Curaçá.

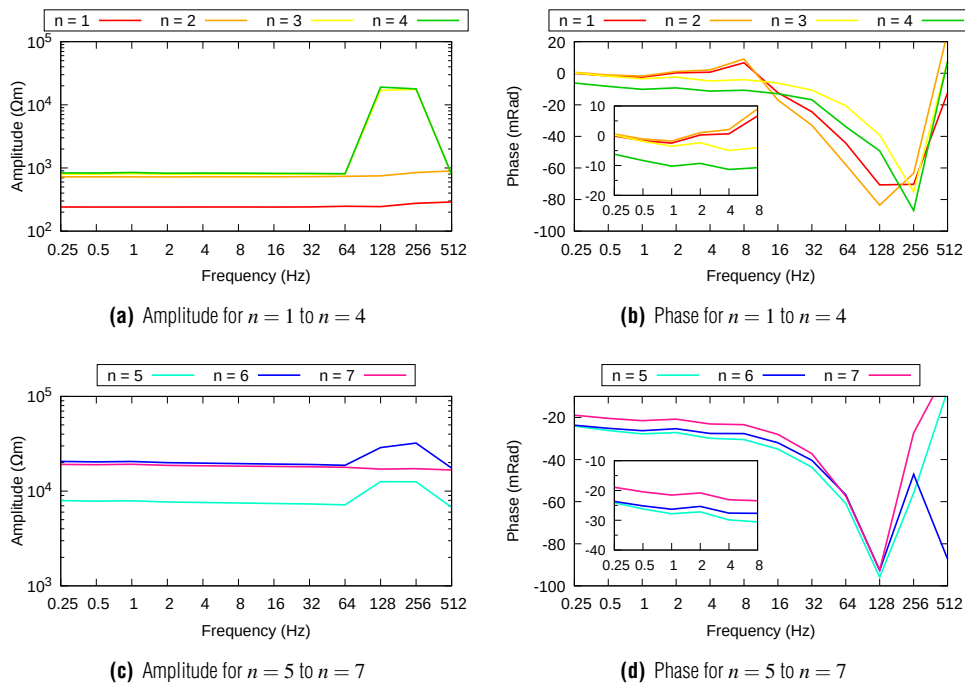


Figure 8 – Spectra of the modulus and the phase of ρ_a for SIP data of one transmitter station of the profile in the Sussuarana area of the Copper District of Vale do Curaçá.

the resistivity with depth. Besides that, depending on how much the polarization affects ρ_a in each separation, there may be a decrease in amplitude with frequency. The phase data is able to better detail variations in the polarization properties of the layers by means of a considerable negative displacement.

The deposits of Vermelhos and Baixa Funda show similar behavior of the phase data with a reduced IP effect at low frequencies. On the other hand, a stronger IP effect is visualized in the Sussuarana phase data.

In summary, the procedure of forward and inverse modelling of the mutual impedance to determine ρ_a allowed to understand its spectral behavior considering the interaction between EMC intrinsic to geophysical acquisition and SIP effect attributed to one or more layers of the 1D Earth model. Thus, applications of this analysis to real data of the Copper District of Vale do Curaçá allowed to distinguish between induction, dominant at the highest frequency values, and SIP, variable with depth and frequency.

The determination of ρ_a is the starting point for the future step of polarization parameters estimation, which leads to the characterization of mineralized bodies in subsurface.

ACKNOWLEDGEMENTS

The authors acknowledge the fellowship from CNPq and CAPES.

REFERENCES

BARRETO AN & DIAS CA. 2014. Fluid salinity, clay content, and permeability of rocks determined through complex resistivity partition fraction decomposition. *Geophysics*, 79(5): D333–D347.

ÇAGLAR I. 2000. A method to remove electromagnetic coupling from induced polarization data for an "exponential" Earth model. *Pure and Applied Geophysics*, 157(10): 1729–1748.

DIAS CA. 2000. Developments in a model to describe low-frequency electrical polarization of rocks. *Geophysics*, 65(2): 437–451.

FULLAGAR PK, ZHOU B & BOURNE B. 2000. EM-coupling removal from time-domain IP data. *Exploration Geophysics*, 31(1/2): 134–139.

MENKE W. 1989. *Geophysical data analysis: Discrete inverse theory*. Academic Press, INC, 289 pp.

MILLETT FB. 1967. Electromagnetic coupling of collinear dipoles on a uniform half-space. *Mining Geophysics*, 2: 401–419.

MOCITAIBA LSR, SAMPAIO EES & DE LIMA OAL. 2017. Effect of coupling noise on the interpretation of results of electromagnetic horizontal sounding and modeling. *Studia Geophysica et Geodaetica*, 61(4): 801–825.

NOCEDAL J & WRIGHT S. 2006. *Numerical optimization*. Springer Science & Business Media, 664 pp.

PELTON WH, WARD SH, HALLOF PG, SILL WR & NELSON PH. 1978. Mineral discrimination and removal of inductive coupling with multifrequency IP. *Geophysics*, 43(3): 588–609.

SAMPAIO EES, SANTOS AB & SATO HK. 1998. Spectral induced polarization and mineral discrimination. In: *SEG Technical Program Expanded Abstracts 1998*, p. 740–743. Society of Exploration Geophysicists.

WYNN JC & ZONGE KL. 1977. Electromagnetic Coupling. *Geophysical Prospecting*, 25(1): 29–51.

XIANG J, JONES NB, CHENG D & SCHLINDWEIN FS. 2002. A new method to discriminate between a valid IP response and EM coupling effects. *Geophysical Prospecting*, 50(6): 565–576.

Recebido em 25 agosto, 2018 / Aceito em 4 outubro, 2018

Received on August 25, 2018 / accepted on October 4, 2018